

A&A manuscript no.
(will be inserted by hand later)

Your thesaurus codes are:
06 (08.03.3 08.01.2 08.18.1 08.05.3 10.15.2)

Ca II activity and rotation in F-K evolved stars[★]

L. Pasquini¹, J.R. de Medeiros², and L. Girardi^{3,4}

¹ European Southern Observatory, Karl-Schwarzschild-Strasse 2, 85748 Garching bei München
email: lpasquin@eso.org

² Departamento de Física, Universidade Federal do Rio Grande do Norte, 59072-970, Natal, RN, Brazil
email: renan@dfe.ufrn.br

³ Max-Planck-Institut für Astrophysik, Karl-Schwarzschild-Strasse 1, 85748 Garching bei München

⁴ Present address: Dipartimento di Astronomia, Vicolo dell' Osservatorio 5, I-35122 Padova, Italy

Received : Accepted

Abstract. Ca II H and K high resolution observations for 60 evolved stars in the field and in 5 open clusters are presented. From these spectra chromospheric fluxes are derived, and a *homogeneous* sample of more than 100 giants is built adding data from the literature. In addition, for most stars, rotational velocities were derived from CORAVEL observations. By comparing chromospheric emission in the cluster stars we confirm the results of Pasquini and Brocato (1992): chromospheric activity depends on the stellar effective temperature, *and* mass, when intermediate mass stars ($M \sim 4M_{\odot}$) are considered. The Hyades and the Praesepe clump giants show the same level of activity, as expected from stars with similar masses and effective temperatures. A difference of up to 0.4 dex in the chromospheric fluxes among the Hyades giants is recorded and this sets a clear limit to the intrinsic spread of stellar activity in evolved giants. These differences in otherwise very similar stars are likely due to stellar cycles and/or differences in the stellar initial angular momentum. Among the field stars none of the giants with $(V-R)_{\circ} < 0.4$ and Ia supergiants observed shows a signature of Ca II activity; this can be due either to the real absence of a chromosphere, but also to other causes which preclude the appearance of Ca II reversal.

By analyzing the whole sample we find that chromospheric activity scales linearly with stellar rotational velocity and a high power of stellar effective temperature: $F'_k \propto T_{\text{eff}}^{7.7} (V\text{sini})^{0.9}$. This result can be interpreted as the effect of two chromospheric components of different nature: one mechanical and one magnetic.

Alternatively, by using the Hipparcos parallaxes and evolutionary tracks, we divide the sample according to the stellar masses, and we follow the objects along an evolu-

tionary track. For each range of masses activity can simply be expressed as a function of *only one parameter*: either the T_{eff} or the angular rotation Ω , with laws $F'_k \sim \Omega^{\alpha}$, because angular velocity decreases with effective temperature along an evolutionary track.

By using the evolutionary tracks and the observed $V\text{sini}$ we investigate the evolution of the angular momentum for evolved stars in the range 1-5 M_{\odot} . For the 1.6-3 solar mass stars the data are consistent with the $I\Omega = \text{const}$ law while lower and higher masses follow a law similar to $I\Omega^2 = \text{const}$, where I is the computed stellar momentum of inertia. We find it intriguing that $V\text{sini}$ remains almost constant for $1M_{\odot}$ stars along their evolution; if a similar behavior is shared by Pop II stars, this could explain the relatively high degree of activity observed in Pop II giants.

Finally, through the use of models, we have verified the consistency of the $F'_k \propto \Omega^{\alpha}$ and the $I\Omega^{\beta} = \text{Const}$ laws derived, finding an excellent agreement.

This representation, albeit crude (the models do not consider, for instance, mass losses) represents the evolution of Ca II activity and of the angular momentum in a satisfactory way in most of the portion of H-R diagram analyzed. Different predictions could be tested with observations in selected clusters.

Key words: Stars: Chromospheric Activity- Stars: Rotation- Stars: Evolution Open Clusters: Hyades, Praesepe, IC4651, NGC 2516, NGC 6067

1. Introduction

The study of activity in the external layers of evolved stars is a quite exciting topic, which still needs firm answers to a number of questions. We do not really know how these chromospheres are powered, and what is the precise relationship between the presence of chromospheres and mass losses, with the interesting implications this may

Send offprint requests to: L. Pasquini

[★] Based on observations collected at ESO, La Silla. Tables 1-3 are only available in electronic form at the CDS via anonymous ftp to cdsarc.u-strasbg.fr (130.79.128.5) or via <http://cdsweb.u-strasbg.fr/Abstract.html>

have for stellar evolution (see e.g. Cacciari and Freeman 1983, Dupree et al. 1992).

In main sequence stars stellar activity is linked to stellar rotational velocity and to the evolution of the angular momentum (i.e. Pallavicini et al. 1981, Noyes et al. 1984); this last quantity, often neglected in stellar evolutionary theory, is becoming more and more relevant in several aspects, for instance when extra mixing mechanisms are required to explain the evolution of elements like Li, Be and C (see, i.e. Zahn 1992, Charbonnel and Do Nascimento 1998). In general, by studying both chromospheres and angular momentum evolution of evolved stars we also aim at better understanding convection, which is one of the most critical aspects in the modeling of the stellar interior.

In this work we have derived chromospheric fluxes based on high resolution spectroscopy in the K line of Ca II. In addition for almost all stars we have derived stellar rotational velocities; we also use the Hipparcos parallaxes to place the stars in the H-R diagram and we finally use theoretical evolutionary models to estimate stellar masses and to interpret the observed data. In addition to stars in the field we have observed 15 giants belonging to 5 open clusters of different turn-off masses, and we use these data to guide the interpretation of the field stars.

2. Observations and Sample

The Ca II observations were obtained at ESO, La Silla in several observing runs in the years 1990-1994. Most observations were obtained at the ESO 1.52m with the Echelec spectrograph (Lindgren 1989), while CASPEC at the ESO 3.6m (Randich and Pasquini 1997) was used to observe the giants in the open clusters IC 4651 and NGC 6067; for both configurations the resolving power obtained was similar, with $R \sim 22000$.

Data reduction was performed by using the echelle context of the MIDAS package; special care was taken in observing several early type stars, to correct properly for the blaze function of the spectrographs, using the recipes described in Pasquini (1992). In the case of the CASPEC observations of NGC 6067, a quite reddened cluster, one early type star belonging to the cluster was observed. This spectrum allowed us to eliminate the strong IS Ca II K line which would otherwise have heavily contaminated our spectra. The spectrum of the early star was fitted, leaving the narrow interstellar absorption line at its position. By dividing the late type star spectra by the early type one, the IS Ca II is therefore eliminated. One example is shown in Figure 1, where the spectrum of the giant CPD-537416 is shown after the correction for the IS line (continuous line) and before (dashed line). The strong IS line, if not considered, would not only alter the chromospheric flux of the cool giants, but also the K line core asymmetry.

The full sample analyzed in this work consists of three different groups:

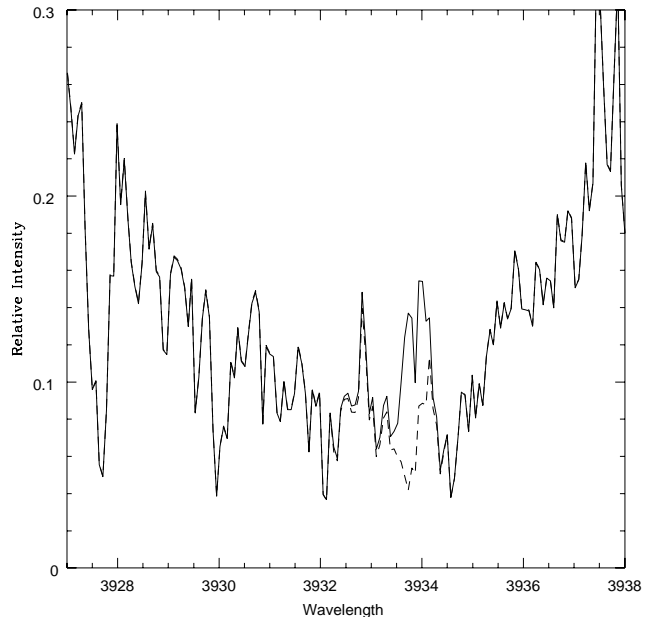


Fig. 1. The Ca II core spectrum of the giant CPD-537416 in NGC6067 is shown, before the correction for the IS Ca II (dashed line) and after (continuous line). Note the change in the asymmetry of the line core

- Stars published by Pasquini and Brocato (1992, hereafter PB92); for these stars CORAVEL rotational velocities and Hipparcos parallaxes are now available.
- 15 Stars belonging to 5 clusters, selected with the aim of covering the largest possible range of ages and turn-off masses. In addition, we also make use of the M67 data from Dupree et al. 1999.
- 45 new Ca II observations of field giants, all of them with measured CORAVEL rotational velocities.

The sample is not complete in any aspect. Most stars were selected because of their bright apparent magnitude, in addition in the new observations several hot giants were observed, because this region in the H-R diagram was not well covered in previous studies. We emphasize, however, that stars were selected neither on the basis of their previously known rotational velocity nor activity level; we should not have therefore inserted any bias with respect to these quantities.

3. Data Analysis

For the sample stars, we aim at determining several quantities: chromospheric fluxes, rotational velocities, stellar effective temperatures and absolute magnitudes.

In addition, for our analysis it is essential to have estimates of the stellar masses. To this end we make use of several evolutionary tracks of solar metallicity computed with the updated Padua code (Girardi et al. 2000). The

momentum of inertia I has been computed for each of the evolutionary points along the tracks. For this study, no mass losses were considered; we note however that for the low and intermediate mass stars we do not expect mass losses to modify substantially I (and therefore our results) at least if a standard Reimers (1975) mass loss law is assumed (see section 4.4 below).

For all stars Ca II K line chromospheric fluxes are computed following the calibrations of Pasquini et al. (1988) and Linsky et al. (1979), and effective temperatures are derived for all stars following the calibration of Pasquini et al. (1990). More recent T_{eff} temperature calibrations exist, nevertheless the Pasquini et al. (1990) calibration has the advantage that it is based on the V-R (Johnson) color, which is the same used to compute the stellar chromospheric fluxes; since most of our analysis is based on relative scales, this will help in reducing systematic effects. Note also that the effective temperatures derived are used exclusively to infer stellar masses and rotational periods; changes in the temperature scale may therefore have some impact on the correlation coefficient derived, but they will not influence our main conclusions.

Absolute magnitudes were derived by using Hipparcos parallaxes, reddening is relevant only for some bright giants and supergiants (Pasquini et al. 1990); $e(V-R)$ was estimated on the basis of Johnson (1966), then the law $e(B-V)=0.66 e(V-R)$ was applied and finally absolute visual magnitudes were derived by using the standard absorption law $A(V)=3.1 e(B-V)$.

Since from our spectra Wilson-Bappu (1957) magnitudes can be derived and these magnitudes were used in the previous, pre-Hipparcos studies, we have computed Wilson-Bappu M_v for all stars, and compared them with the Hipparcos ones. Most of the observed stars are within 200 pc, and their Hipparcos parallaxes are therefore very accurate. In Figure 2 the comparison between absolute magnitude as computed by using the Wilson-Bappu law following Lutz (1970) (as applied in PB92) and the Hipparcos parallaxes is shown. A systematic trend is present: the W-B law gives systematically brighter magnitudes than Hipparcos. We think that a re-calibration of the Wilson Bappu law with Hipparcos stars would become a powerful tool to infer the absolute magnitude of late type stars.

As far as rotational velocities are concerned, the $Vsini$ measurements were derived from the CORAVEL survey of de Medeiros and Mayor (1999), but several stars have $Vsini$ measured by Gray and coworkers (Gray 1982, 1983, Gray and Pallavicini 1989, Gray and Toner 1987, Gray and Nagar 1985); the claimed accuracy for both analyses is in the range of 0.5-1 km/sec. Since for ~ 50 stars both CORAVEL and Gray rotational velocities are available, a comparison can be performed, and it is shown in Figure 3. For most stars the agreement between the two sets of measurements is excellent, within 1 km/sec, but discrepancies much larger than the quoted errors exist: the

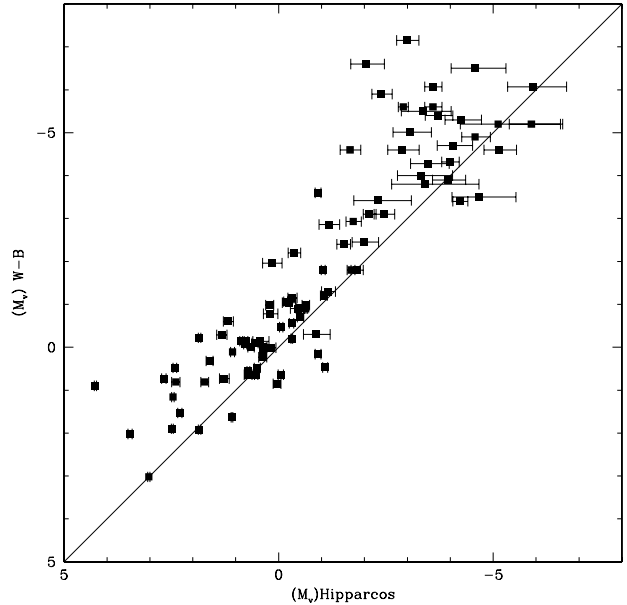


Fig. 2. Comparison between the Visual absolute magnitudes as derived from Hipparcos and from the Wilson Bappu law, following Lutz (1970)

results are consistent with the results of De Medeiros and Mayor (1999) who found for a larger sample of giants and subgiants: $Vsini(COR) = -1.15 + 1.18 \times Vsini(Gray)$; since the CORAVEL measurements are available for all stars, we will adopt them in the following, ensuring an homogeneous data set.

3.1. Previously Published stars

PB92 investigated the dependence of Ca II activity from several stellar parameters, using Ca II observations of quality comparable with the present one, and using the same calibration, V-R temperature scale, bolometric corrections by Flower (1977), and determining the stellar reddening following Johnson(1966).

Table 1 contains the updated PB92 data. The differences from PB92 are that absolute magnitudes are now based on the Hipparcos parallaxes and the CORAVEL rotational velocities have been added, as well as a binarity flag, which indicates if the stars are likely single (S), spectroscopic binary (SB) and with known orbit (SBO).

From the PB92 sample, for only 5 stars $Vsini$ measurements were unavailable (all of spectral class M) and these stars are not considered in the present subsample, which therefore consists of 60 stars. Rotational velocities from Gray and collaborators are given, when available. G refers to Gray (1982, 1983), GN to Gray and Nagar (1985), GT to Gray and Toner (1987), GP to Gray and Pallavicini (1989).

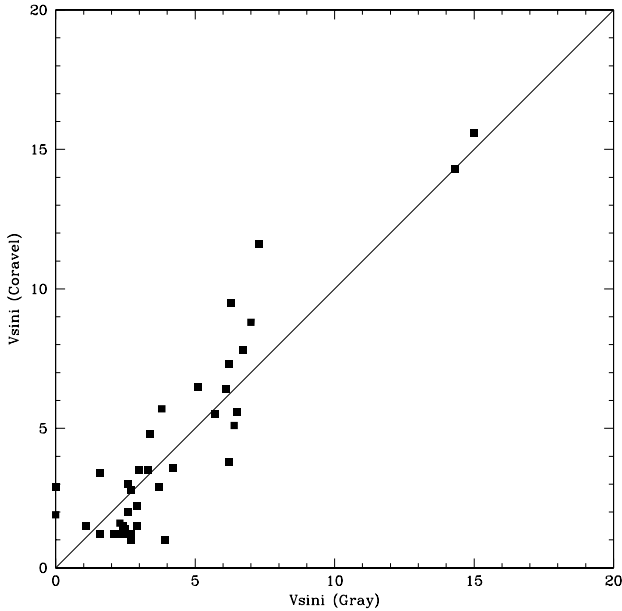


Fig. 3. Comparison between CORAVEL and Gray V_{sini} for the sample stars common to the two groups

3.2. Cluster stars

In addition to the field stars, vital information may be obtained by analyzing stars belonging to open clusters, for which basic stellar parameters are better constrained. As part of this project, 15 giants belonging to 5 clusters were observed; the clusters are (ordered as decreasing turn-off masses): NGC 2516, NGC 6067, Praesepe, Hyades, and IC4651. The cluster stars were analyzed in the same way as the field stars, and the same effective temperature scale was adopted.

In Table 2, the data on the observed clusters are presented; turn-off masses, reddening and distance modulus are taken from Meynet and Mermilliod (1993) for NGC 2516 ($E(B-V)=0.12$, turn-off= $4.3M_{\odot}$), NGC 6067 ($E(B-V)=0.314$, turn-off= $4.5M_{\odot}$) and IC 4651 ($E(B-V)=0.08$, turn-off= $1.4M_{\odot}$). For Hyades and Praesepe, distances are derived directly from Hipparcos parallaxes; $E(B-V)=0$ and turn-off= $2.05M_{\odot}$ have been assumed. A_k refers to the ratio between the Ca II K line core area and the pseudo-continuum at 3950\AA (Pasquini et al. 1988), while $A(50)$ refers to the same area, divided by the 3925-3975 bandpass (Linsky et al. 1979).

3.3. New Field stars

The last subsample includes the new Echelec observations of field stars. These observations were acquired to enlarge the PB92 sample, both to obtain more stars with measured rotational velocities and to explore Ca II activity among bright (and hot) giants and supergiants, a region

of the H-R diagram poorly investigated in previous studies.

Table 3 summarizes the basic data for this subsample; column names are as in Table 1, while A_k and $A(50)$ are as in Table 2. It is worth noticing that for 12 stars no signature of Ca II K line core reversal is observed. All these stars are either rather hot (with $(V-R)_o \leq 0.4$), or belonging to the Ia supergiant class. We will return to this point in the discussion.

4. Discussion

4.1. Cluster Stars

The obvious advantage of observing stars in clusters is to eliminate the uncertainties always present in the stellar parameters of field stars. Stars belonging to a cluster can for most purposes be approximated to a homogeneous sample in age, chemical composition, and, when referring to the evolved stars, masses as well. In addition, when observing one cluster, the magnitude and temperature sequence of the stars is usually well defined, at least on a *relative* scale.

We recall that, since the cluster star observations are processed in the same way as the field stars, they form an homogeneous sample with them; this implies that it should be possible to extend the results of the cluster stars to the field ones.

In Figure 4 Ca II fluxes are shown as a function of the stellar effective temperature. Stars from different clusters are marked with different symbols. In this Figure, in addition to the data of Table 2, the sequence of giants from M67 (Dupree et al. 1999) is added. The M67 data were acquired at a similar spectral resolution and analyzed in a similar way to the present sample. A different Ca II calibration was used, and when the difference between the calibrations is taken into account, the results are in excellent agreement (Dupree et al. 1999); the M67 Ca II fluxes from Dupree et al. (1999) have been corrected to be homogeneous with the present analysis.

Figure 4 confirms the well known trend between stellar activity and effective temperature in evolved stars: the higher the temperature, the higher the chromospheric emission. In addition it can be noticed that:

1. The Hyades giants show a spread of chromospheric fluxes of up to 0.4 dex. Since this difference is known to be largely caused by stellar cycles (Baliunas and Vaughan 1985, see also Stern et al. 1995 for a discussion on the X-ray emission), this first result provides an estimate of the cosmic spread of chromospheric activity in evolved stars: a difference of a few dex can be found even in otherwise almost identical stars.
2. The Hyades and Praesepe giants, which have similar ages, temperatures and masses, also show the same mean level of chromospheric activity. This is reassuring, because it indicates that it may indeed be possible

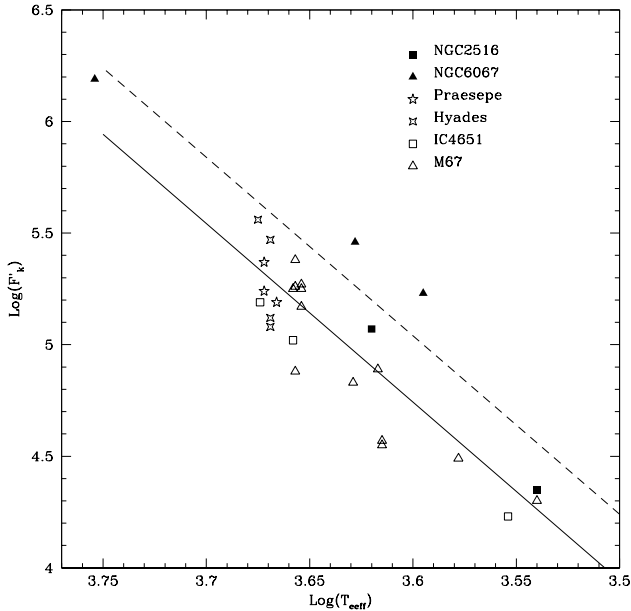


Fig. 4. $\text{Log } F'_k$ vs. effective temperature for the observed open clusters giants. Stars from different cluster are marked with different symbols. The M67 data of Dupree et al. (1999) are also included in the Figure.

to represent (within the cosmic spread of point 1) chromospheric activity as a function of macroscopic stellar parameters. The fact that the chromospheric levels are the same among Praesepe and Hyades giants is also in very good agreement with the finding by Randich and Schmitt (1995) of a similar X-ray luminosity among the evolved stars of these two clusters.

3. The lower mass RGB stars (IC4651 and M67) form a well defined, *narrow* sequence with emission slightly lower than the Hyades and Praesepe clump giants, while the M67 clump stars (located at $\log T_{eff} \sim 3.66$) have fluxes similar to the younger Hyades and Praesepe.
4. It is well known that when field stars are plotted in the same activity-temperature diagram, they show a large spread. In Figure 4 we may observe how, introducing the $\sim 4.3 M_{\odot}$ stars from NGC 2516 and 6067, the spread is enhanced, in that the more massive stars tend to show higher levels of chromospheric activity for a given T_{eff} than the lower mass stars. In the same Figure the $F'_k \propto T_{eff}^8 \times M$ relationship found by PB92 is also shown. The continuous line represents what is expected for the Hyades and Praesepe clusters according to this law: the data are well reproduced. In addition the broken line gives the predictions for 4 M_{\odot} stars. Clearly, the high mass clusters confirm these predictions.

4.2. Field Stars

The H-R diagram of the field stars observed is given in Figure 5. In this diagram the evolutionary tracks for several masses (1, 1.3, 1.6 2, 3, and 5 M_{\odot}) are also shown, together with the observed cluster stars (including the M67 stars from Dupree et al. 1999). To make the Figure more readable, cluster stars are grouped in 3 symbols, according to the cluster turn-off masses: stars of NGC 2516 and 6067 as filled pentagons, stars of Hyades and Praesepe as filled squares, stars from M67 and IC4651 as filled triangles. In Figure 5 the continuous lines refer to the RGB, while the broken lines represent the 1 and 1.6 M_{\odot} HB.

Clearly the field stars span a large range in mass and evolutionary status. We also note the good agreement between the cluster turn-off masses as given in Table 2 and those indicated by the evolutionary tracks: differences can be ascribed to the photometry adopted, set of tracks used and to differences in the effective temperature scales adopted. We emphasize that a detailed study of the colour magnitude diagram of these clusters is *beyond the scope of the present work*, and that for our purposes the agreement shown in Figure 5 is excellent. As expected, there is some degeneracy in allocating masses in the region of the yellow giants, where He-burning Hyades-like and M67-clump like stars tend to group. The spread of stars in this region in fact reflects the age dispersion (and to a lower extent the metallicity dispersion) among the giants in the solar neighborhood (Girardi et al. 1998).

In Figure 5 we only plot those stars of Table 3 with chromospheric emission determination. From Table 3 it emerges clearly that the stars with no detected chromospheric emission are confined to two well determined groups: class Ia supergiants and stars with $(V-R)$ smaller than ~ 0.4 . It is tempting to say that these stars define regions where chromospheric activity is not present, for instance because they are so hot that they do not possess a subphotospheric convective zone. However this cannot be determined uniquely on the basis of the Ca II data, because several causes may make the detection of Ca II emission impossible in these stars:

- For the hot stars high rotational velocities will tend to smear out the Ca II core, and make the detection of the Ca II minima impossible; in addition high photospheric contribution at 3933 Å will also make the contrast in the Ca II core very shallow.
- For the three Ia supergiants, we know that these stars have large line broadening, with atmospheres not in static equilibrium. This line broadening may wipe out the Ca II core, making its detection impossible. It would not be surprising, however, if the atmospheres (or chromospheres, if present at all) of these stars would be very different from those of the other late-type giants forming the sample (see e.g. Achmad et al. 1997).

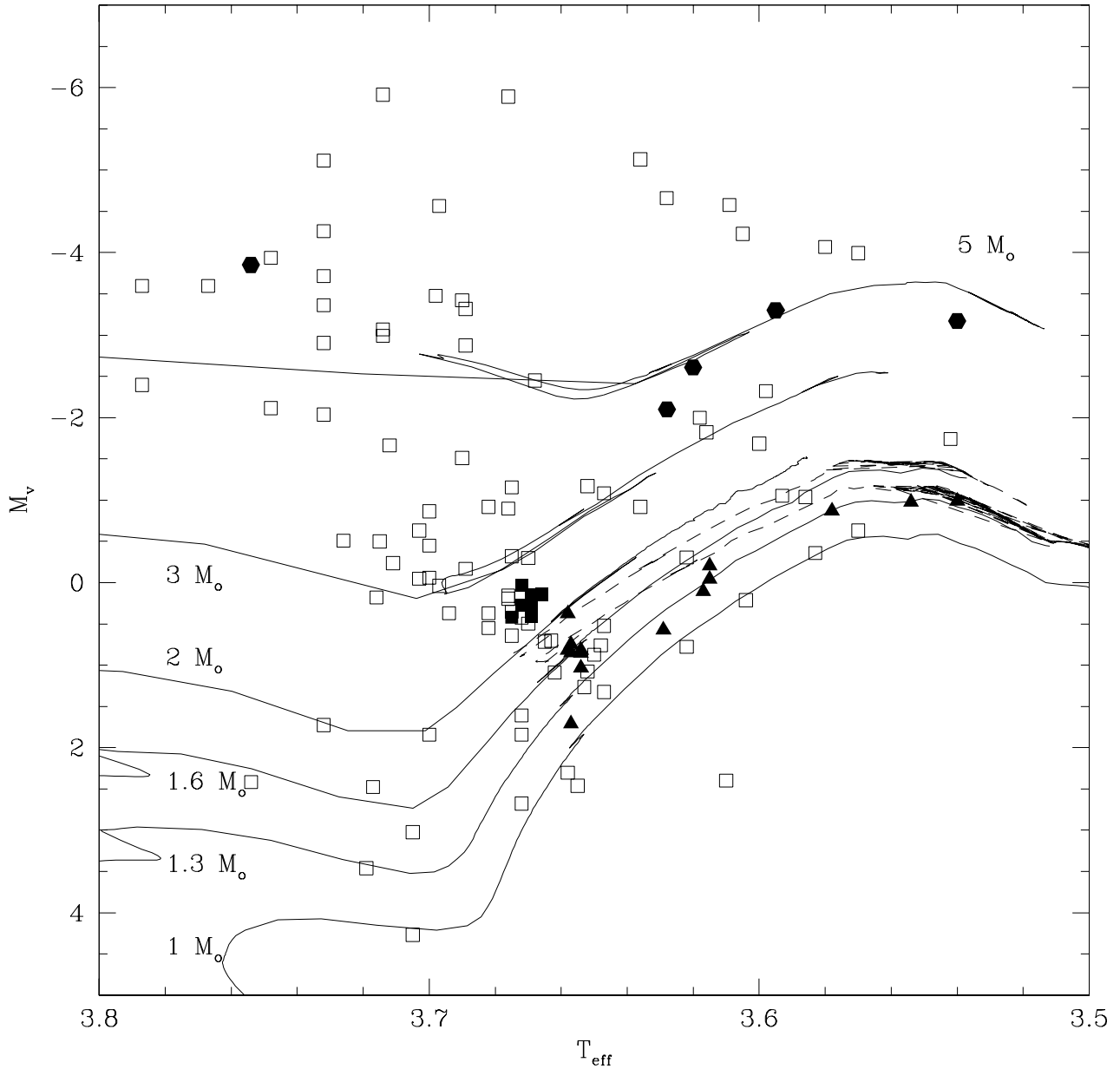


Fig. 5. H-R diagram for the sample stars. Cluster stars have different symbols, depending on the cluster turnoff mass: filled triangles IC4651 and M67 stars; filled squares: Hyades and Praesepe; filled pentagons: NGC2516 and 6067 stars; open squares: field stars

In Figures 6a,b chromospheric fluxes are shown for all field stars as a function of effective temperature and measured rotational velocity, respectively. Clearly a strong dependence of chromospheric activity on both quantities is present, although with a large scatter.

In Figure 6b two active stars have low rotational velocities. Since our sample contains ~ 100 stars, some of the objects are expected to have very high inclination angles,

and therefore these high activity, low $V \sin i$ stars are likely to be pole-on candidates.

$V \sin i$ and T_{eff} are on the other hand only slightly correlated in our sample, as shown in Figure 7; this allows us to fit activity with both quantities, obtaining:

$$F'_k \propto T_{\text{eff}}^\alpha V \sin i^\beta$$

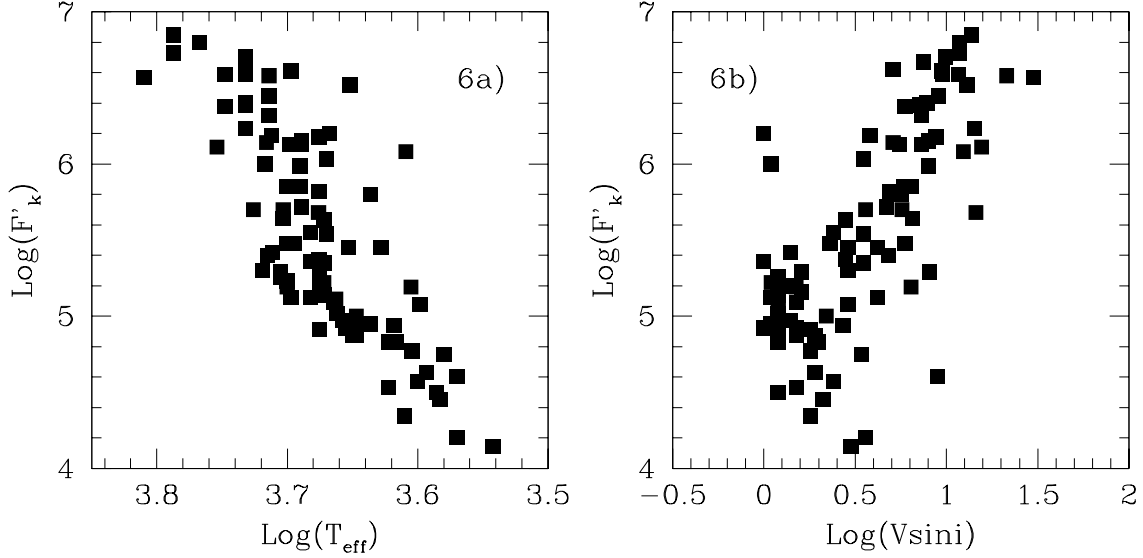


Fig. 6. Figure 6a: $\text{Log } F'_k$ vs T_{eff} for the sample stars; Figure 6b: $\text{Log } F'_k$ vs $Vsini$

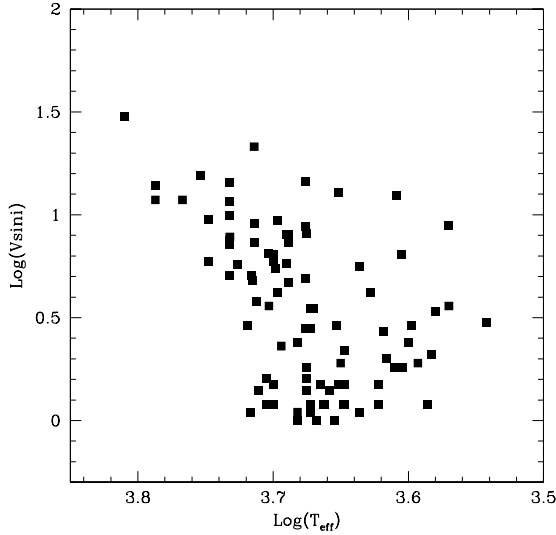


Fig. 7. $Vsini$ vs T_{eff} for the sample stars.

with $\alpha = 8.01 \pm 0.7$ and $\beta = 0.8 \pm 0.1$ and a standard deviation of 0.32 dex. Eliminating from the sample the two pole-on candidates of Figure 6b the fit changes only marginally ($\alpha = 7.7$ and $\beta = 0.9$) with a standard deviation of 0.29 dex. When considering the intrinsic chromospheric variability and all the uncertainties involved in the analysis (including the *sin i*), this can be considered a good representation of the data set. A similar dependence was

found by Strassmeier et al. (1994) by analyzing a sample containing normal and active giants.

When comparing this result with that of PB92, we find the same strong dependence of activity on T_{eff} , and a similar scatter in the final relationship. The fact that PB92 found a linear dependence of chromospheric activity on stellar mass and now a similar dependence on $Vsini$ is found, suggests that $Vsini$ should scale with the stellar mass: for the same effective temperature, more massive giants should have higher rotational velocities.

One immediate explanation for the observed correlation is to assume that the dependence on T_{eff} and $Vsini$ represents two well separated mechanisms: the dependence on T_{eff} being a component related to the stellar structure, and the $Vsini$ term representing an additional source of chromospheric heating, likely of magnetic origin. This scheme has been proposed in the past by several authors (see e.g. Rutten and Pylyser 1988 and references therein), and it is natural to associate the 'temperature' component with that generated by acoustic heating (see e.g. Cuntz et al. 1997). The acoustic theory has been developed in the last 20 years, and some of the most recent works (Buchholz et al. 1998) predict an activity-temperature dependence very close to the one observed. It is not clear to the authors if, for instance, any dependence of acoustic heating should be expected with stellar mass, due to the different internal structure of the stars sharing the same effective temperature.

The presence of stellar cycles in the Hyades giants as well as the measurements of Ca II variability induced by rotational modulation could on the other hand ques-

tion the relevance of the acoustic heating mechanism and these observed phenomena suggest that acoustic heating may represent only a small fraction of the overall chromospheric heating budget. In the specific case of the Hyades giants for instance, the differences observed would indicate that the magnetic part is at least 4 times higher than the acoustic contribution. The data of the Hyades giants, however tell us also something else: that even if a correlation between activity and $Vsini$ is found, a simple correlation can only have a limited range of accuracy: indeed among the Hyades giants, the difference in measured $Vsini$ is rather small (cfr. Table 2), and their difference in activity cannot likely be ascribed directly to a difference in stellar rotation. This indicates that any activity - rotation relationship, while it can provide with a broad agreement with the observations, it may hide rather complex physical mechanisms, possibly similar to those in force in the sun.

A different approach considers that in the presence of a composite sample, we can divide the sample according to the stellar masses and follow the evolution of the chromospheric activity along each of the evolutionary tracks. For instance it is clear that while a star evolves along its track, its rotational velocity will also evolve, giving a dependence of rotational velocity from effective temperature and the plot of figure 7 could therefore be the result of merging many stars with different masses and evolutionary histories in the same diagram.

In the following we will analyze the data by studying the possible relationship between activity and angular momentum evolution, making use of the evolutionary tracks. A somewhat similar approach was adopted by Rutten and Pylyser (1988); these authors found that the post main sequence evolution of angular momentum and of stellar activity could be, at least qualitatively, explained in terms of angular momentum conservation for the most massive stars, while for stars of $2 M_{\odot}$ or lower, this law would predict a much too high activity (and rotation rate) for stars having intermediate temperatures. The advantage of using Hipparcos based parallaxes, homogeneously determined chromospheric fluxes and stellar rotational velocities, together with the information coming from the clusters, should provide new hints on this topic.

We have therefore subdivided our sample according to the evolutionary tracks: if stars are closer than 0.01 in $\text{Log}(T_{eff})$ and 0.3 in M_v to the 1, 1.3, 1.6, and $2 M_{\odot}$ evolutionary tracks, they were given the respective masses. For more massive stars the M_v requirements were relaxed: for $3 M_{\odot}$ stars all objects within M_v ($-0.3 + 0.7$) from the track have been given $3 M_{\odot}$, while all stars above the $5 M_{\odot}$ curve and 0.7 magnitudes below it were considered as $5 M_{\odot}$ stars. Clearly this division suffers from some limitations: for example several stars will be common to two subsamples; in addition, since in this subdivision we have considered only the RGB, in the region of the yellow giants we will attribute higher masses to some clump low mass

stars; finally, the $5 M_{\odot}$ subsample will be more composite than the others.

4.3. Empirical relationships for different masses

Under the hypothesis that all stars belonging to a subsample represent different evolutionary stages of objects having otherwise similar characteristics, linear fits of $\text{Log } F'_k$ vs different quantities performed for the different subsamples will tell us how chromospheric activity will evolve for the stars of a given age (or turnoff mass). We have performed fits of the following form: $F'_k \propto X^{\alpha}$, where X can be either the rotational velocity $Vsini$, the angular velocity Ω or the effective temperature T_{eff} . The results of the fits are given in Table 4, together with the dispersions.

We can immediately notice that, when subdividing the stars in mass ranges, for the $1.3-3 M_{\odot}$ samples, the Ca II emission can rather well be represented as a function of $Vsini$, without any need for an additional parameter, with a dependence of activity on $Vsini$ close to 1. For the $1 M_{\odot}$ Ca II does not depend on rotational velocity. The $1 M_{\odot}$ case is very interesting because, as we will see later, taking the data at face value, a rather peculiar angular momentum evolution is required. For the $5 M_{\odot}$, while stellar activity depends strongly on T_{eff} , it does not depend on $Vsini$.

Since $Vsini$ is a quantity which involves the stellar radius, rotational periods could be a more appropriate parameter to represent any rotationally induced effect. We have computed for each star the stellar radius from the data in Tables 1,2,3 and derived periods. The results of the fits are also given in Table 4 and the diagrams are shown in Figure 8. With the exception of the $5 M_{\odot}$ stars, very good fits can be obtained by using this parameter. Finally, good fits for all our subsamples can be obtained by using T_{eff} as governing parameter.

From Table 4 several points emerge:

a) That the representation of the chromospheric flux is better obtained as a function of Ω than $Vsini$

b) That the Ca II fluxes can be well represented as a function of the angular velocity only, but for stars of $\sim 5 M_{\odot}$ and above the fit is rather poor. A large slope is required for these stars. A clear drop in the relationship is clearly present in Figure 8 when the coolest supergiants are considered: these stars show *higher* rotational velocities (or lower Ca II fluxes) than expected from extrapolating the trend given by the hotter stars.

c) While the dependence on T_{eff} can be acceptable for most mass intervals, it may be difficult to explain how this dependence should strongly change in slope among the different subsamples if T_{eff} was the only relevant parameter.

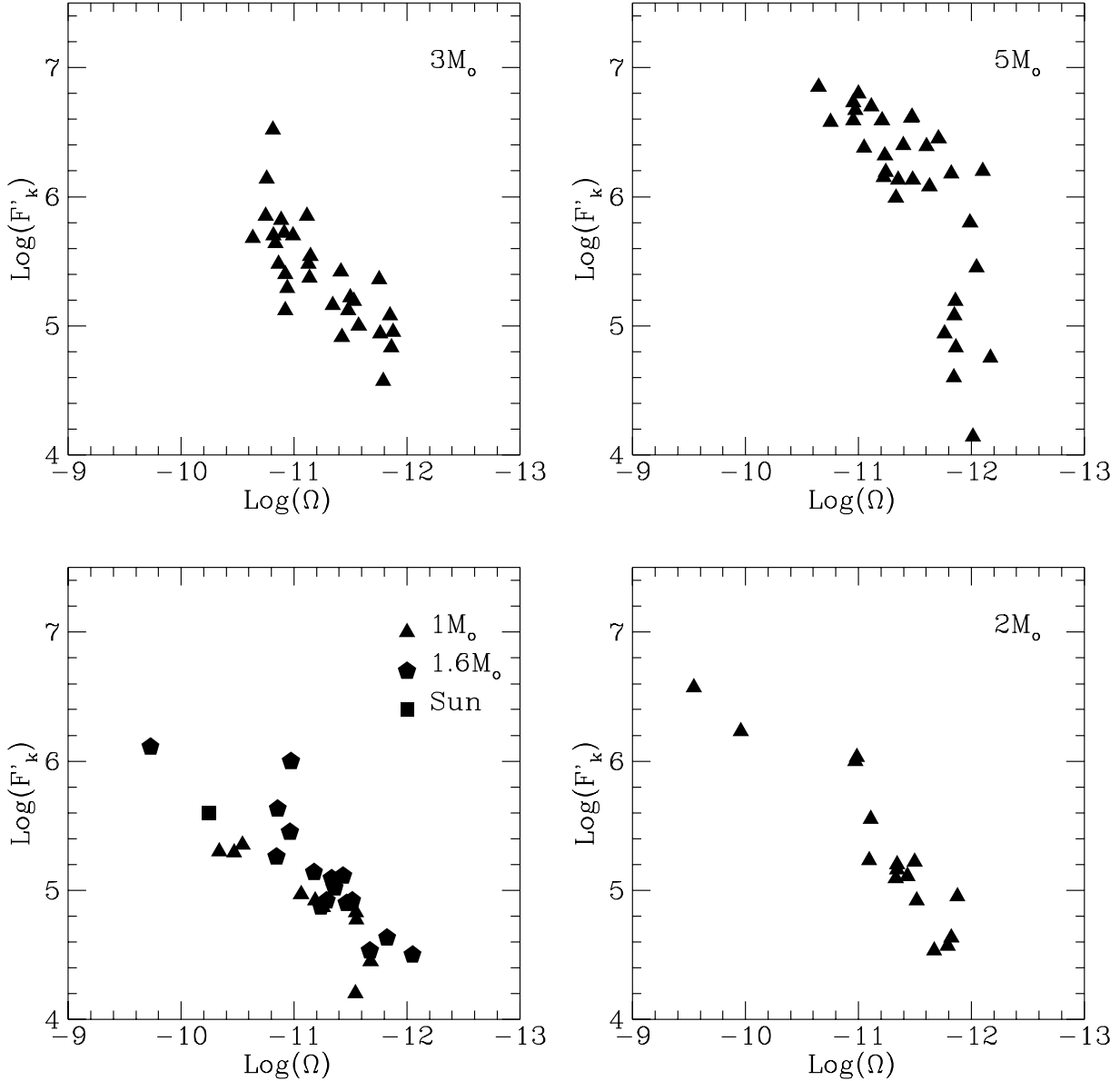


Fig. 8. $\text{Log } F'_k$ vs. Ω for the different mass subsamples. In the first panel both 1 and 1.6 M_\odot stars are given, with different symbols. The sun is also plotted as a filled square

4.4. Angular Momentum Evolution

The measured $V \sin i$ and the attribution of masses allow also a preliminary analysis of the evolution of the stellar angular momentum. We have computed from the Padua models the momentum of inertia I of the stars along the

evolutionary tracks. For spherically symmetric distribution of density $\rho(r)$ I is given by:

$$\frac{8\pi}{3} \int_0^R \rho(r) r^4 dr \quad (1)$$

where r is the radial coordinate and R the stellar radius. We recall that the adopted models do not include mass losses, angular momentum redistribution from the interior or braking. In the following we will not perform fits to the

Table 4. Empirical relationships $\text{Log } F'_k$ found when analyzing separately the sample stars with different masses.

Function	α 1M $_{\odot}$	σ 1M $_{\odot}$	α 1.6M $_{\odot}$	σ 1.6M $_{\odot}$	α 2M $_{\odot}$	σ 2M $_{\odot}$	α 3M $_{\odot}$	σ 3M $_{\odot}$	α 5M $_{\odot}$	σ 5M $_{\odot}$
Vsini	0.0	0.37	0.92	0.38	1.03	0.42	0.87	0.31	1.56	0.59
Ω	0.65	0.18	0.70	0.24	0.86	0.23	0.89	0.26	1.3	0.48
T _{eff}	7.5	0.15	9.99	0.2	10.35	0.26	6.76	0.34	10.5	0.27

observed $V_{\text{sin}i}$, rather we will verify if the observed $V_{\text{sin}i}$ distribution can be reproduced in terms of simple scaling laws of the form $I\Omega^{\beta} = \text{Const}$.

4.4.1. Low Mass stars

Figure 9a,b show the rotational velocities for the 1 and 1.6 M $_{\odot}$ stars respectively. The observed $V_{\text{sin}i}$ of table 1 and 2 have been multiplied by $4/\pi$ to take into account the projectional effects.

The first striking point is that, if taken at face values, the $V_{\text{sin}i}$ of the 1 M $_{\odot}$ stars is independent of the stellar effective temperature and therefore of their evolutionary status. This is at odds with the intuitive picture, from which we would expect that the stars slow down rather quickly after they leave the main sequence and that further deceleration could happen if magnetic braking is at work. In Figures 9a,b the lines represent what is expected from the simplest hypothesis:

$$I\Omega = \text{Const}(M)$$

$$\text{or } V = V_o \times 1/I$$

The 1 M $_{\odot}$ curve has been adjusted to reproduce the solar equatorial velocity of 2 km/sec (continuous line in Figure 9a), while for the 1.6 M $_{\odot}$ stars the curve has been adjusted to reproduce the mean distribution of the giants.

Clearly, this simple law does not work for the 1 M $_{\odot}$ stars: giants rotate too fast to obey the angular momentum conservation law. Of course one could consider that the solar zero point is wrong and that a typical solar type star has a rotational velocity as large as twice that of the Sun; but even when considering this case (broken line in Figure 9a) the conservation of angular momentum would predict far too low rotational velocities for the giants. Only with a law of the type $I\Omega^2 = \text{Const}$ can the data points be reproduced, as is shown by the dashed dotted line in Figure 9a, which represents the behavior of this law. It is interesting to observe, however, that in case activity and rotational velocities were related, these relatively high $V_{\text{sin}i}$ for the low mass stars would explain the relatively high level of activity observed among the globular clusters giants (Dupree et al. 1990, 1994). But we have to stress that the $V_{\text{sin}i}$ values measured in these stars are typically of a few km/sec, therefore measurement uncertainties (systematics in particular) could in this regime play a crucial role.

Pending more and more accurate data on 1 M $_{\odot}$ giants, we can conclude that the angular momentum evolution of

these low mass stars does not follow a $I\Omega = \text{Const}$ law, but possibly a more steep one. From the physical point of view it is difficult to explain this behavior: possibly large mass losses in the RGB phase (which are also required for the interpretation of the color-magnitude diagrams of globular clusters) with winds not suffering magnetic backing could explain part of this behavior, but we would expect these mass losses, if at all, to act mostly towards the coolest part of the RGB only.

For the 1.6 M $_{\odot}$ stars the situation is different: the conservation of angular momentum law reproduces very well most stars. To better look into this point, in Figure 9b the rotational velocities of three 1.3-1.6 M $_{\odot}$ stars having measured rotational periods are shown as starred points (Choi et al. 1995). Finally, in the same Figure the filled squares represent the CORAVEL $V_{\text{sin}i}$ of stars belonging to the open cluster NGC 3680 (mean of 8 turn-off single stars and mean of 4 single giants, corrected by $4/\pi$, Nordstrom et al. 1996,1997): the agreement between the prediction of the constant angular momentum law derived for the field stars and the NGC 3680 points is impressive.

It is worth recalling that there is a basic structural difference between the 1 and the 1.6 M $_{\odot}$ stars of figure 9a and 9b: the low mass stars present a radiative nucleus and a convective envelope on the main sequence, whereas the opposite situation is found in the more massive stars. This may also produce relevant differences in the evolution of the stellar rotational velocity.

4.4.2. Intermediate mass stars (2-3 M $_{\odot}$)

Figures 10 a,b show the 2 and 3 M $_{\odot}$ subsamples with, superimposed, the results obtained by assuming angular momentum conservation. The agreement is very good. As in Figure 9b starred points are V as derived from the Choi et al. (1995) periods. The filled squares represent the Hyades and Praesepe measured $V_{\text{sin}i}$. It is worth noticing that out of the Choi et al. stars, 3 are belong to Praesepe and 1 to the Hyades; for these stars we can therefore compare the $V_{\text{sin}i}$ with the V derived from the observed periods. $V_{\text{sin}i}$ values are systematically lower than the V derived from the periods. The Hyades and Praesepe giants have a mean $V_{\text{sin}i}$ of 1.74 km/sec, while for the 4 Praesepe and Hyades giants from Choi the mean V is of 5.4 km/sec. This result indicate that the Coravel $V_{\text{sin}i}$ may slightly underestimate the $V_{\text{sin}i}$ for these stars, in line with the offset between Coravel and Gray measurements quoted above.

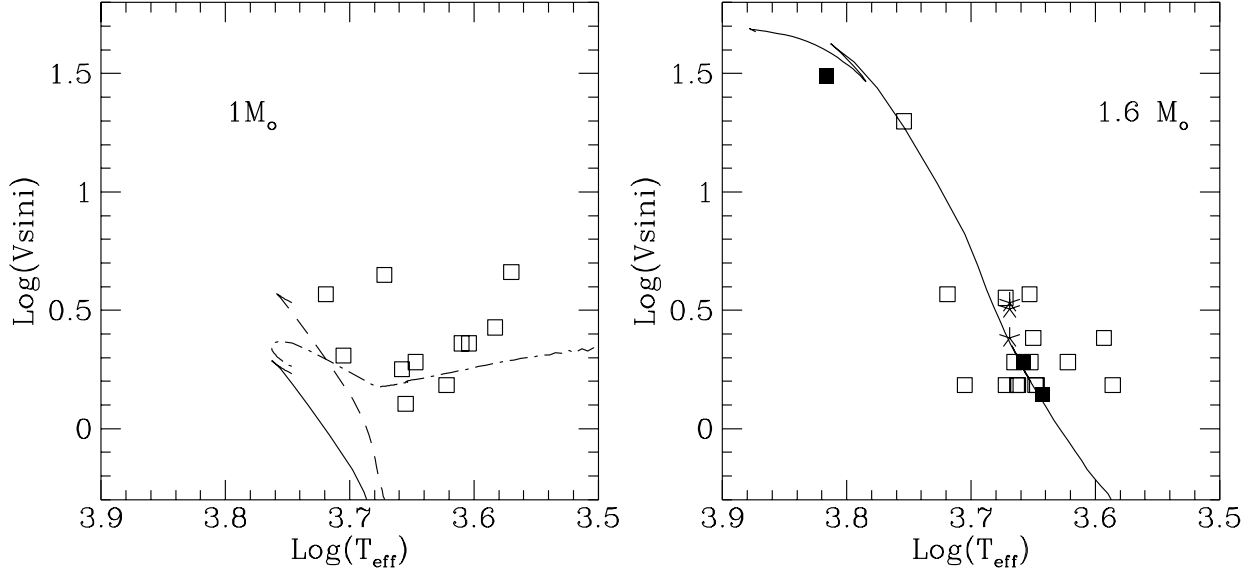


Fig. 9. $V_{\text{ sini}}$ vs. T_{eff} for the low mass subsamples. Figure 9a: for $1M_{\odot}$ stars. The continuous line represents what is expected in the case $I\Omega=\text{Const}$. The dashed-dotted line represents what is expected if a $I\Omega^2=\text{Const}$ law would hold. Figure 9b: Same as 9a), but for $1.6 M_{\odot}$ stars. Rotational velocities derived from period measurements (Choi et al. 1995) are given as starred; the filled dots represent the mean rotational velocities measured in the NGC 3680 stars: 8 (single) turn-off and 4 giants.

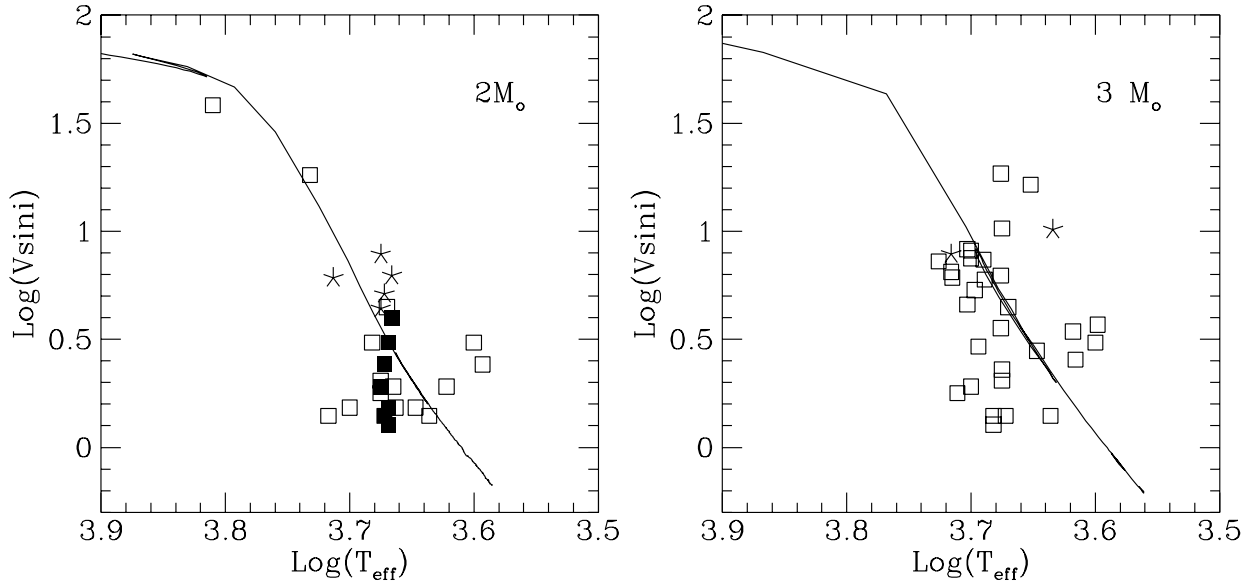


Fig. 10. $V_{\text{ sini}}$ vs. T_{eff} for the intermediate mass subsamples. Figure 10a: for $2M_{\odot}$ stars. The continuous line represents what is expected in the case $I\Omega=\text{Const}$. Rotational velocities derived from period measurements (Choi et al.) are given as starred; the filled dots represent the mean rotational velocities measured in the NGC 3680 stars: 8 (single) turn-off and 4 giants and the values for the Hyades and Praesepe stars of Table 2. Figure 10b: the same for the $3 M_{\odot}$ stars

The angular momentum conservation law would predict a $V \sim 65$ km/sec for the Hyades turn-off stars, which is comparable to, but lower than the observed mean turn-off velocity of 100 ± 50 km/sec (Gaipe 1993). Although we cannot consider this discrepancy as significant (in fact the Hyades turnoff value would be perfectly reproduced if a systematic effect is present and the line was passing through the Choi et al. (1995) points of Figure 10a), still the difference could be due to the simplification adopted in our model; a factor two slow down between turn-off and giant stars is predicted for instance by models adopting internal angular momentum redistribution (Endal and Sofia 1979).

4.4.3. High mass stars ($5M_{\odot}$)

Figure 11 shows the behavior of the rotational velocity vs. effective temperature for the $5M_{\odot}$ stars. Obviously the $\Omega = \text{Const}$ law (continuous line) does not represent the data. As for the $1M_{\odot}$ stars the distribution of rotational velocities requires a much steeper dependence on the angular velocity. In the same Figure the $\Omega^2 = \text{Const}$ law is given, which approximates much better the observations. As found for the Ca II analysis in the previous chapter, the cool supergiants seem to rotate too fast with respect to what is predicted by their hotter 'precursors'. We do not have any explanation for this phenomenon, we caution only that for these stars the nominal uncertainty in $V_{\text{ sini}}$ is likely underestimated, since in these stars other line broadening mechanisms may be comparable or superior to those induced by $V_{\text{ sini}}$.

4.5. Consistency

Before deriving any conclusion, we believe that it is important to perform a cross check of the previous analysis. We shall in this section outline a summary of the analysis previously performed.

We have first seen how F'_k can be well fitted as a function of Ω^α , with Ω derived from $V_{\text{ sini}}$, M_{Bol} and T_{eff} as given in tables 1,2,3. As a second step we have investigated the dependence of the observed $V_{\text{ sini}}$ on the $I\omega^\beta = \text{Const}$ scaling law by using the momentum of inertia I as computed by theoretical models, finding that the data are consistent with $\beta=2$ for the 1 and the $5M_{\odot}$ stars, and $\beta=1$ for the 1.6-3 M_{\odot} stars. Combining these results we expect that for each subsample the derived Ca II chromospheric fluxes should depend on the momentum of inertia I (as computed by the models) according to $F'_k \propto I^{-\alpha/\beta}$, where α for the different subsamples is given in Table 4 and $\beta=1$ or 2 depending on the stellar mass subsamples.

We have therefore used the models and the previously determined exponents to verify this consistency and the results are shown in Figures 12a-e for the different mass subsamples. As can readily be seen, the results are very satisfactory, confirming therefore the consistency and the

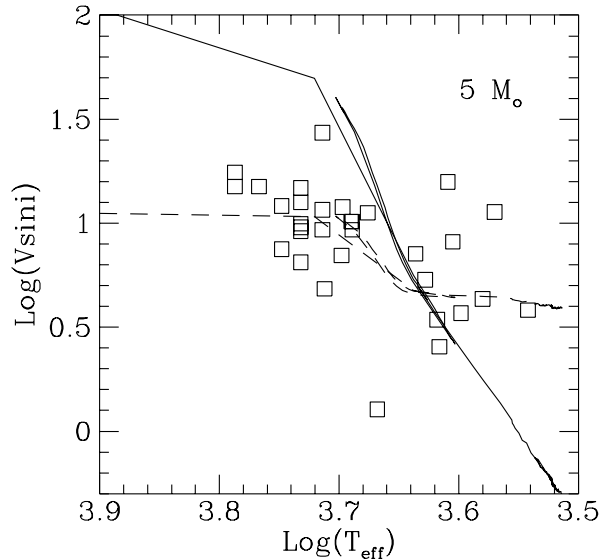


Fig. 11. $V_{\text{ sini}}$ vs. T_{eff} for the $5M_{\odot}$ stars. The continuous line represents what is expected in the case $\Omega = \text{Const}$. The dashed-dotted line represents what is expected if a $\Omega^2 = \text{Const}$ law would hold.

quality of our analysis. We find the results in Figure 12a-e very encouraging, although several improvements could be performed in future studies.

This analysis holds for our sample stars, whose angular momentum behavior is not dominated by those phenomena, like tidal locking, which determine the dynamic behavior in short period binaries. For those cases rotational periods should instead be taken explicitly into account.

5. Conclusions

By providing a large, *homogeneous* sample of Ca II chromospheric fluxes *and* rotational velocities for field *and* cluster F-K giants, thanks to the use of *Hipparcos* accurate parallaxes and *evolutionary tracks*, we have found first approximation laws which govern chromospheric activity and angular momentum evolution in F-K giants and supergiants. In particular:

1. Hot giants and Ia supergiants do not show Ca II emission. We cannot conclude from the Ca II only if this is due to the absence of a chromosphere or to other factors (high $V_{\text{ sini}}$, large turbulence)
2. When considering young clusters, the results are in agreement with what is observed by PB92: for a given effective temperature more massive stars tend to have higher chromospheric fluxes than low mass stars.
3. Hyades and Praesepe giants show the same *mean* level of chromospheric activity, as expected for stars having the same mass and effective temperature.

4. However Hyades stars show a spread of up to 0.5 dex in chromospheric fluxes. This difference shows that stellar cycles produce some 'cosmic' scatter among stars which are otherwise very similar. This scatter would limit our prediction capabilities even in the absence of measurement errors.
5. When analyzing the whole sample the Ca II fluxes can be well represented by $F'_k \propto T_{eff}^{7.7} \times V \sin i^{0.9}$.
6. On dividing the sample into stars of different masses by using evolutionary tracks, we find that we can represent F'_k for all subsamples but the 5 M_{\odot} stars as a function of the angular velocity: $F'_k \propto \Omega^{\alpha}$. Also, in each subsample F'_k can be well represented as a function of the stellar effective temperature T_{eff} (cfr. Table 4)
7. By using the momentum of inertia I as deduced by theoretical models we have verified that the observed rotational velocities can be represented by simple $I\Omega^{\beta} = \text{Const}$ laws. 1.6-3 M_{\odot} giants are consistent with angular momentum conservation law ($\beta=1$), while for the 1 and 5 M_{\odot} giants a steeper, $\beta=2$ law seems more appropriate. (We caution, however, that for different reasons these two samples may be heavily affected by systematic errors in their $V \sin i$ measurements).
8. The $V \sin i$ data for 1 M_{\odot} stars do not show any dependence on the stellar evolutionary status. This result is at odds with the intuitive expectations.
9. Finally we have checked the consistency of our analysis and we have been able to reproduce the observed Ca II chromospheric fluxes F'_k as a function of the theoretical momentum of inertia using the results from the above analysis: $F'_k \propto I^{-\alpha/\beta}$.

As far as the mechanism governing stellar activity in giant stars is concerned, our analysis shows how, with two macroscopic parameters, it is possible to determine the level of chromospheric activity in evolved stars. This can be explained in two alternative ways:

a) Chromospheres are powered by two mechanisms: one dependent on the stellar rotational velocity and one on the stellar effective temperature.

b) Evolved stars of the same mass tend to behave similarly, having similar angular momentum for a given position on the evolutionary tracks. The angular momentum evolution is however different for stars of different masses and angular velocity and mass are the only parameters determining the level of activity.

We stress that some of the present uncertainties could be dissipated by observing subgiants and giants in well populated clusters. A full self consistent analysis (e.g. including fitting of the C-M diagram) with the theoretical models would reveal which of the above interpretations is correct. Also, measurements of rotational periods in many more giants and supergiants will be fundamental in assessing systematic uncertainties in the $V \sin i$ measurements.

Acknowledgements. A large part of this work was prepared during the stay of LP at UFRN in Natal. This work has been possible thanks to the ESO DGDF and Brazilian agency CNPq grants. The work of LG was funded by the Alexander von Humboldt stiftung. We are grateful to L. Achmad for his help in the data reduction and P. Bristow for a careful reading of the manuscript.

References

- Achmad, L., Lamers, H.J.G.L.M., Pasquini, L. 1997, A&A 320, 196
- Anthony-Twarog, B.J., Mukherjee, K., Twarog, B.A., Caldwell, N. 1988, AJ 95, 1453
- Baliunas, S.L., Vaughan, A.H. 1985 ARA&A 23, 379
- Buchholz, B., Ulmschneider, P., Cuntz, M. 1998, ApJ 494, 700
- Cacciari, C., Freeman, K.C. 1983, ApJ 268, 185
- Charbonnel, C., do Nascimento, J.D. Jr. 1998 A&A, 336, 915
- Choi, H-J, Soon, W., Donahue, R.A., Baliunas, S.A., Henry, G. 1995, PASP 107, 744
- De Medeiros, J.R., Mayor, M. 1999, A&ASS, 139, 433
- Dupree, A.K. et al. 1990, ApJ 361, L9
- Dupree, A.K., et al. 1994, ApJ 421, 542
- Dupree, A.K., Whitney, B.A., Pasquini, L. 1999, ApJ, 520, 751
- Endal, A.S., Sofia, S. 1979, ApJ 232, 531
- Flower, P.J. 1977, A&A 54, 163
- Gaige', Y. 1993, A&A 269, 267
- Girardi, L., Groenewegen, M.A.T., Weiss, A., Salaris, M. 1998, MNRAS 301, 149
- Girardi, L., Bressan, A., Bertelli, G., Chiosi, C. 2000, A&ASS 141, 371
- Gray, D.F. 1982, ApJ 262, 682
- Gray, D.F. 1983, PASP 95, 181
- Gray, D.F., Nagar, P. 1985, ApJ 298, 756
- Gray, D.F., Toner, C.G. 1987, ApJ 322, 322
- Gray, D.F., Pallavicini, R. 1989, PASP 101, 695
- Johnson, H.L. 1966, ARA&A 4,193
- Lidgren, H., Gilliotte, A. 1989, "ECHELEC User Manual" (ESO)
- Lindoff, U. 1972, A&ASS 7, 231
- Lindoff, U. 1973, A&ASS 9, 229
- Linsky, J.L., Worden, S.P., McClintock, W., Robertson, R.M. 1979, ApJS 41, 47
- Lutz, T.E. 1970, AJ 75, 1007
- Meynet, G., Mermilliod, J-C, Maeder, A. 1993, A&ASS 98, 477
- Nördstrom, B., Andersen, J., Andersen, M.I. 1996, A&ASS 98, 477
- Nördstrom, B., Andersen, J., Andersen, M.I. 1996, A&AS 322, 460
- Noyes, R., et al. 1984 ApJ 279, 763
- Pallavicini, R., et al. 1981, ApJ 248, 279
- Pasquini, L. Pallavicini, R., Pakull, M 1988, A&A 191, 266
- Pasquini, L. Pallavicini, R., Dravins, D. 1989, A&A 213, 261
- Pasquini, L., Brocato, E. 1992, A&A 266, 340 (PB92)
- Pasquini, L. 1992, A&A 266, 347
- Randich, S., Schmitt, J.H.M.M. 1995, A&A 298, 115
- Randich, S., Pasquini, L. 1997, "CASPEC User Manual" (ESO)
- Reimers, D. 1975, Mem. Soc. R. Sci. Liege, ser. 6, vol. 8, 369
- Rutten, R.G.M., Pylyser, E. 1988, A&A 191, 227

- Stern, R. A., Schmitt, J.H.M.M., Kahabka, P.T. 1995, ApJ 448, 683
- Strassmeier, K.G., Handler, G., Paunzen, E., Rauth, M. 1994, A&A 281, 395
- Thackeray A.D., Wesselink, A.F., Harding, G.A. 1962, MNRAS 124, 445;
- Wilson, Bappu, V. 1957, ApJ 125, 661
- Zahn, J.P. 1992, A&A 265, 115

Table 1. PB92 stars. Column 1: HD number; Column 2: Spectral Type; Column 3: Binaricity flag; Column 4: Effective Temperature; Column 5: M_v (Hipparcos); Column 6: M_{Bol} ; Column 7: Log of Ca II chromospheric fluxes; Column 8: $Vsini$ CORAVEL; Column 9: $Vsini$ (Gray and collaborators); Column 10: Color excess $e(V-R)$

HD	Sp. Type	Bin	T_{eff}	M_v	M_{Bol}	LogF'_k	$Vsini$	$Vsini(\text{Gr})$	$e(V-R)$
2261	K0III	SB	3.647	0.52	0.03	4.92	1.2	2.1 GP	
4128	K0IIICh-1H	S	3.670	-0.30	-0.67	5.54	3.5	3.0 G	
9270	G7IIIa	S	3.675	-1.16	-1.53	5.29	8.1		
11937	G8IIIbCNIV	S	3.717	2.48	2.24	6.00	1.1		
13611	G6II-IIIC	SB	3.700	-0.87	-1.07	5.19	1.5		
16522	G8III	S	3.682	0.37	-0.04	5.12	1.1		0.03
17652	G8IIIb	S	3.675	0.64	0.27	5.20	1.4		0.05
21120	G6IIIFe-1	SB	3.700	-0.44	-0.70	5.48	5.9		
27256	G8II-III	SB	3.689	-0.17	-0.35	5.72	4.7		
29139	K5III	S	3.570	-0.63	-1.73	4.20	3.6		
36079	G5II	SB?	3.703	-0.63	-0.79	5.64	6.5	5.1 G	
39364	G8IIIwkCN	S	3.652	1.08	-0.63	4.92	1.5		
48329	G8Ib	SB	3.676	-5.89	-6.13	6.18	8.8	7.0 GT	0.37
50310	K0III	SBO	3.647	-1.08	-1.57	5.00	2.2	2.9 GP	0.06
50778	K4III	S	3.583	-0.36	-1.36	4.45	2.1		
52497	G5IIa-Ib	S	3.690	-3.42	-3.60	5.99	8		0.02
57146	G2Ib	S	3.732	-3.36	-3.40	6.70	9.9		0.12
57623	F6II	S	3.767	-3.60	-3.56	6.80	11.8		0.22
59890	G3Ib	S	3.697	-4.57	-4.71	6.61	9.4		0.12
61064	F6III	SB?	3.810	-1.18	-1.28	6.57	30.1		
62345	G8IIIa	S	3.675	0.35	-0.02	5.16	1.6		
63700	G3Ib	SB	3.714	-5.91	-6.02	6.45	9.1		0.25
65228	F7II	S	3.787	-2.34	-2.33	6.85	13.8		0.14
67594	G2Ib	S	3.732	-5.12	-5.16	6.39	7.2		0.15
68752	G5II	S	3.689	-3.32	-3.50	6.13	7.3		0.09
71129	K3III+B2V	S	3.609	-4.58	-5.23	6.08	12.4		
74395	G1Ib	S	3.732	-2.04	-2.08	6.67	7.5		0.07
77258	G8K-III+A	SBO	3.670	0.50	0.12	6.03	3.5		
81797	K3II-III	S	3.600	-1.69	-2.39	4.57	2.4		
84441	G1II	S	3.748	-2.12	-2.12	6.38	5.9		0.14
89485	G7IIICN-I	S	3.682	-0.92	-1.12	5.36	1	2.7 G	
92449	G2-3Ib	S	3.732	-3.72	-3.76	6.62	5.1		0.17
93497	G5III+G2V	S	3.700	-0.06	-0.30	5.85	6.4	6.1 GP	
98430	G8III-IV	SB	3.675	-0.32	-0.67	4.91	1.8		
100407	G7III	S	3.682	0.55	0.20	5.55	2.4		
102350	G5Ib-II	S	3.690	-1.51	-1.81	5.85	5.8		
105707	K2.5IIIa	S	3.616	-1.82	-2.50	4.83	2	2.6 GP	
109379	G5II	S	3.726	-0.51	-0.66	5.70	5.7	3.8 G	
111028	K1III-IV	S	3.610	2.397	1.717	4.34	1.8		
113226	G8IIIab	S	3.694	0.37	0.089	5.48	2.3		
115659	G8IIIa	S	3.703	-0.047	-0.29	5.70	3.6	4.2 GP	
116243	G6II	S	3.697	0.037	-0.22	5.12	4.2		
123139	K0IIIb	S	3.663	0.70	0.27	5.11	1.2		
124897	K1IIIbCN1	S	3.622	-0.31	-0.99	4.53	1.5	2.4 G	
150798	K2IIb-III	S	3.605	-4.23	-4.90	5.19	6.4		0.13
151680	K2.5III	S	3.622	0.78	0.12	4.83	1.2	2.2 GP	
157999	K2II	SB	3.628	-4.66	-5.15	5.45	4.2		
159181	G2II	SB	3.732	-2.90	-2.94	6.59	11.6	7.3 GT	
162076	G5IV	S	3.653	1.27	0.82	5.45	2.9		
164058	K5III	S	3.586	-1.04	-2.03	4.50	1.2		
168723	K2IIIabC1	S	3.700	1.84	1.59	5.23	1.2	2.7 GN	
171443	K3III-IIb	S	3.604	0.21	-0.61	4.77	1.8		
173764	G5IISBO	S	3.689	-2.88	-3.06	6.15	8		0.1
200905	K4-5Ib-II	SB	3.580	-4.07	-4.83	4.75	3.4	1.6 GT	
204867	G0Ib	S	3.748	-3.94	-3.94	6.59	9.5	6.3 GT	0.1
206778	K2Ib	S	3.636	-5.13	-5.57	5.80	5.6	6.5 GT	0.2
209750	G2Ib	S	3.732	-4.26	-4.30	6.40	7.8	6.7 GT	0.08
211416	K3III	SBO	3.593	-1.05	-1.97	4.63	1.9		
218356	K0II	SB	3.668	-2.45	-2.72	6.20	1	3.9 GT	0.24

Table 2. Cluster data. NCC2516 photometry is from Lindoff (1973), NGC 6067 photometry from Thackeray et al. (1962) IC4651 photometry from Anthony-Twarog et al. (1988), numbers from Lindoff (1972). For reddening and distance modulus, see text. In column 11 V/R gives the ratio between the Violet and Red K2 emission in the line core. V/R<1 may indicate outflows

ID	B-V	B-V _o	V-R	V-R _o	T _{eff}	M _v	A(K)	A(50)	V/R	FKP	FKL	F' _k	Vsini	Clus
HR3120	1.55	1.43	1.03	0.95	3.620	-2.61	.250	.0150	1.02	5.00	5.22	5.07	2.8	2516
HR3153	1.74	1.62	1.44	1.36	3.554	-3.17	.884	.0315	.21	4.41	4.41	4.35	/	2516
CPD-537400	1.10	.79		(.55)	3.759	-3.85	.239	.0119	.83	6.22	6.35	6.19	/	6067
CPD-537344	1.78	1.47		(1.02)	3.595	-3.3	.613	.032	.89	5.17	5.33	5.23	/	6067
CPD-537416	1.55	1.24		(.84)	3.628	-2.1	.300	.0157	.93	5.42	5.57	5.46	/	6067
HD73598	.96	.96	.72	.72	3.672	.03	.120	.0063	/	5.39	5.55	5.37	/	Praes.
HR3428	1.02	1.02	.74	.74	3.666	.14	.103	.0048	1.40	5.27	5.37	5.19	3.1	Praes.
HR3427	.98	.98	.72	.72	3.672	.27	.094	.0050	/	5.29	5.45	5.24	1.1	Praes.
HR1346	.99	.99	.73	.73	3.669	.28	.159	.0079	1.14	5.49	5.62	5.47	1.0	γTau
HR1373	.98	.98	.73	.73	3.669	.41	.081	.0044	1.22	5.19	5.36	5.12	1.2	δTau
HR1409	1.01	1.01	.73	.73	3.669	.15	.075	.0042	1.13	5.16	5.34	5.08	2.4	εTau
HR1411	.95	.95	.71	.71	3.675	.42	.166	.0082	1.0	5.57	5.69	5.56	1.5	θTau
IC4651-56	1.65	1.56		(1.28)	3.554	-.98	.448	.0210	.91	4.23	4.35	4.23	/	
IC4651-37	1.03	.95		(.70)	3.674	.22	.082	.0040	/	5.29	5.41	5.19	/	
IC4651-113	1.13	1.05		(.77)	3.658	.37	.092	.0044	.99	5.12	5.4	5.02	/	

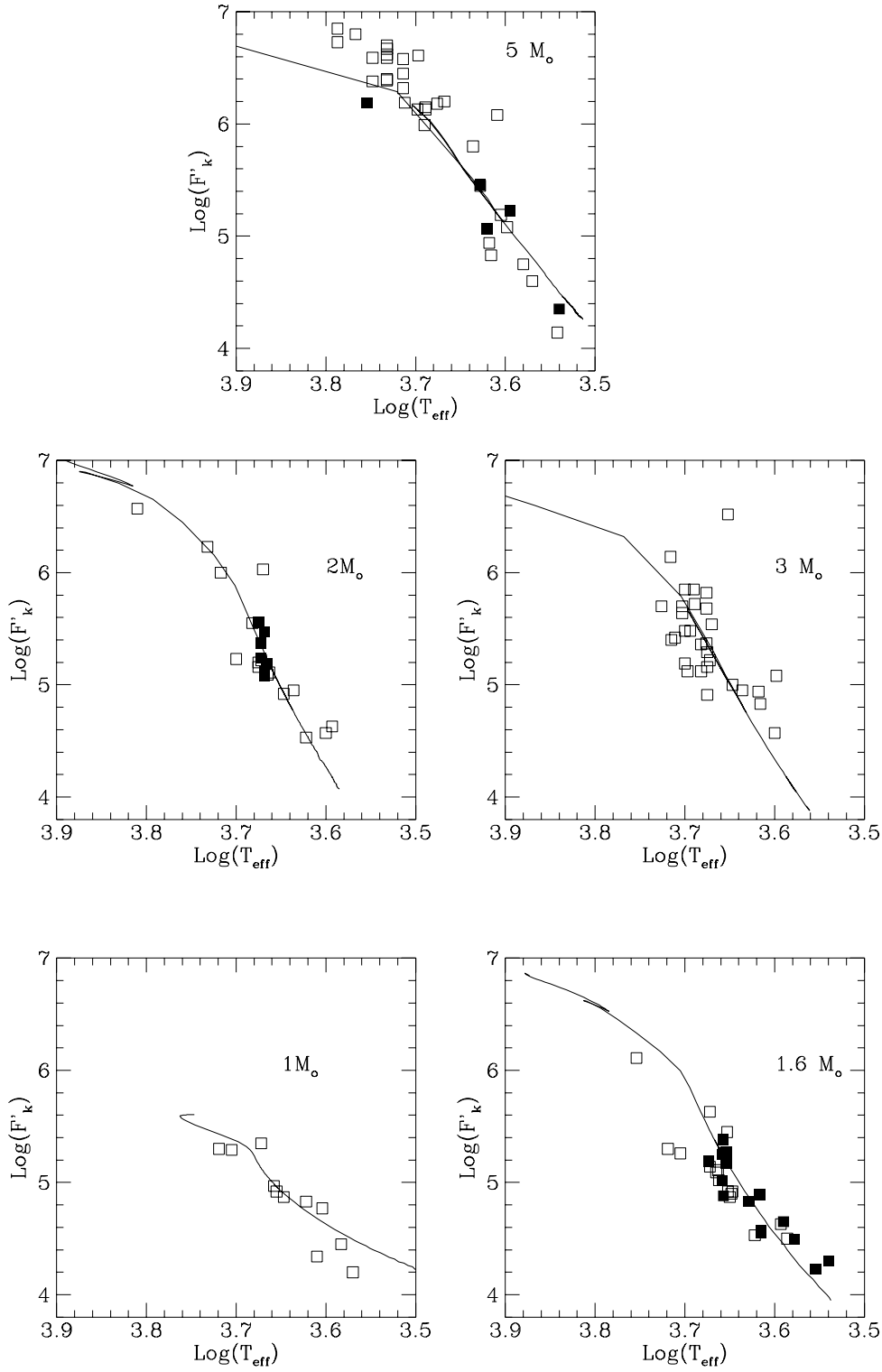


Fig. 12. Verification of the results obtained: the Ca II fluxes $\text{Log } F'_k$ vs T_{eff} diagrams are reproduced by the expected $\log F'_k \propto I^{-\alpha/\beta}$ with α as derived from Table 4 and $\beta=1$ for $1.6\text{-}3 M_{\odot}$ and $\beta=2$ for 1 and $5 M_{\odot}$ (cfr. Figures 9,10,11)

Table 3. New Ca II observations of field stars. Column 1-3 as in Table 1; Column 4: Measured (V-R); Column 5: Adopted (V-R)_o; Column 6: Effective Temperature; Column 7: M_v (Hipparcos) Column 8: M_{Bol}; Column 9: Ak Index; Column 10: A(50) Index; Column 11: K line V/R asymmetry; Column 12: Log Ca II K line chromospheric flux (ergs cm⁻² sec⁻¹ at the stellar surface); Column 13: *Vsini*(CORAVEL); Column 14: *Vsini*(Gray)

HD	Sp. Ty.	Bin	(V-R)	(V-R) _o	T _{eff}	M _v	M _{Bol}	A(K)	A(50)	V/R	LogF _k	VC	VG
496	K0III	S	0.75	0.75	3.665	0.71	0.28	.095	.0046	1.2	5.09	1.5	2.9
30834	K2.5III	S	1.09	(0.96)	3.618	-2.00	-2.68	0.190	.0110	1.04	4.94	2.7	/
47205	K1III	S	0.79	0.79	3.655	2.46	1.99	.080	.0045	1.07	4.92	1	2.7
57623	F6II	S	0.67	(0.45)	3.787	-3.60	-3.52	.345	.018	1.23	6.73	11.8	/
62509	K0III	S	0.75	0.75	3.662	1.09	0.66	.077	.0043	1.08	5.02	1.2	2.5
67228	G1V	S	0.63	0.63	3.719	3.46	3.29	.071	.0031	1.11	5.3	2.9	3.7
78647	K4Ib-I	S	1.24	1.24	3.570	-3.99	-5.19	.743	.0350	0.57	4.6	8.9	/
80230	M1III	S	1.34	1.34	3.542	-1.74	-3.4	.434	.0205	0.44	4.14	3	/
89484	K1III	SB	0.85	0.85	3.636	-0.92	-1.49	.116	.0067	1.0	4.95	1.1	2.6
94481	G4III	S	/	(.69)	3.676	0.16	-0.21	.106	.0052	1.0	5.37	2.8	/
101379	G2III+A	SB	0.79	0.79	3.655	-1.17	-1.66	.316	.0084	/	6.52	12.9	/
101570	G3Ib	SB	0.87	(.63)	3.714	-2.99	-3.09	.962	.0402	1.06	6.58	21.4	/
118219	G6III	S	/	(.70)	3.672	0.42	0.05	.084	.0043	1.1	5.22	1.1	/
121107	G5III	S	/	(.69)	3.676	-0.89	-1.27	.193	.0090	/	5.68	14.5	/
124850	F6III	S	0.5	0.5	3.754	2.42	2.33	.155	.0057	1.06	6.11	15.6	15
126868	G2IV	SB	0.58	0.58	3.732	1.73	1.59	.320	.0130	/	6.23	14.3	14.3
130259	G5III	S	/	(.69)	3.676	0.20	-0.18	.253	.0118	1.02	5.82	4.9	/
138716	K1III-IV	S	0.77	0.77	3.658	2.30	1.85	.080	.0043	1.09	4.97	1.4	2.5
140573	K2III	S	0.81	0.81	3.650	0.87	0.38	.081	.0049	1.13	4.87	1.9	0.
142980	K1IV	S	/	(.82)	3.647	1.33	0.84	.085	.0049	.99	4.87	1.5	1.1
144608	G3II-III	S	0.65	0.65	3.711	-0.24	-0.44	.091	.0045	1.16	5.42	1.4	/
148856	G7IIIa	SBO	0.64	0.64	3.715	-0.50	-0.70	.097	.0049	1.31	5.4	4.8	3.4
161096	K2III	S	0.82	0.82	3.647	0.76	0.27	.085	.0052	1.15	4.9	1.2	1.6
168723	K2III	S	0.70	0.70	3.672	1.84	1.47	.074	.0038	1.13	5.14	1.2	2.7
181391	G8III-IV	SBO	/	(.70)	3.672	1.61	1.24	.149	.0069	1.08	5.63	2.8	2.7
182572	G8IV	S	/	(.66)	3.705	4.27	4.05	.080	.0037	/	5.29	1.6	2.3
188512	G8IV	S	0.66	0.66	3.705	3.03	2.81	.075	.0035	1.1	5.26	1.2	2.2
192876	G3Ib	SB	0.79	(.63)	3.714	-3.07	-3.16	.493	.0239	1.07	6.32	7.3	6.2
196725	K3Ib	S	1.02	1.02	3.598	-2.32	-3.07	.448	.0236	.33	5.08	2.9	0.0
196755	G5IV+K2V	S	/	(.70)	3.672	2.68	2.31	.111	.0050	1.1	5.35	3.5	3.3
203387	G8III	S	0.62	0.62	3.716	0.18	-0.02	.322	.0147	1.08	6.14	5.1	6.4
206859	G5Ib	S	0.80	(.67)	3.698	-3.48	-3.62	.411	.0205	1.00	6.13	5.5	5.7
204075	G4Ib	SB	0.64	0.64	3.712	-1.66	-1.76	.402	.0189	1.22	6.19	3.8	6.2
67523	F6II	/	0.35	0.35		1.41						14.6	/
78791	F9II	/	0.55			-1.25						66.5:	/
79940	F5III	/	0.38	0.38		1.10						/	/
96918	G40-Ia	/	0.87			-7.34						/	/
100261	G30-Ia	/	0.83			-4.91						/	/
101947	G00-Ia	/	0.76			-4.48						/	/
129502	F2 III	SB	0.40	0.40		2.51						4.9/11.2	/
155203	FIII-IVp	/	0.36	0.36		1.61						/	/
174474	A2V	/	/			1.42						/	/
178524	F2II	/	0.34	0.34		-2.77						3.2	/
182835	F2Ib	/	0.51			-8.1						11.5	/
196524	F5IV	/	0.40	0.40		1.26						49.8	/